CFD Analysis of the Effects of Multiple Semicircular Blades on Savonius Rotor Performance

Mohamed Meziane*‡, Mustapha Faqir**, Elhachmi Essadiqi**, Mohammed Fathi Ghanameh**

* Laboratory of Condensed Matter and Renewable Energy, Faculty of Science and Technology, Hassan II University, Casablanca, Morocco

** Université Internationale de Rabat, AERO School, LERMA Laboratory, Rocade Rabat-Salé, 11100 Sala el Jadida, Morocco

(mohamed.meziane@univh2c.ma, mustpha.faqir@uir.ac.ma, elhachmi.essadiqi@uir.ac.ma, fathi.ghannmeh@uir.ac.ma)

‡ Corresponding Author; Mohamed Meziane, Casablanca, Tel: +212 6 42 88 52 14,

mezian.med@gmail.com

Received: xx.xx.xxxx Accepted:xx.xx.xxxx

Abstract- The goal of this work is to simulate and improve the efficiency of an innovative multiple semicircular-bladed Savonius rotor, which is identified as belonging to the vertical axis wind turbine (VAWT) category. It is characterized as a low speed turbine that is simpler and cheaper to build than traditional turbines. This makes it appropriate for generating mechanical energy in lower wind speed regions, and it can be coupled with solar panels in urban agglomerations. The objective of this paper is to compare the aerodynamic characteristics and power efficiency of four different geometries (two-conventional and two-modified rotors) in order to estimate the most efficient design. The proposed Savonius design comprises multiple semicircular blades added to conventional two- and three-bladed Savonius configurations. The comparison of the efficiency in terms of the torque coefficient (C_T) and power coefficient (C_P) of the new system configurations with the conventional ones finds that the multiple semicircular two-bladed Savonius rotor is more efficient than others. An average improvement in the power coefficient of 8.43% is observed for the new configuration compared with the others.

Keywords Savonius rotor, VAWT, Multiple-semicircular Savonius roto, Power coefficient.

1. Introduction

In the last few years, with the rapid development of economic activities, the excessive exploitation of fossil energy sources has led to the decrease of resources and the deterioration of environment. Energy and environmental problems have become huge challenges for governments and scientific community. The use of renewable resources becomes one of the main topics for society. Wind energy is one of the most widely used and fast growing renewable energy resources for large-scale exploitation. It is the most sustainable way to generate electrical power without directly emitting air pollutants. This kind of energy has received growing interest and had resulted in an upward trend of wind power getting more penetration in the grids. The Global Wind Energy Council (GWEC) released a report stating that the cumulative capacity of installed wind power worldwide reached some 596.6 GW by 2018 [1]. China, the US, and Germany are the top three countries, producing 62.5% of the global installed wind capacity. In Uruguay, currently, 97% to 100% of electricity comes from renewable sources, of which 30% is from wind energy.

Wind turbines convert incoming wind kinetic energy into mechanical energy, which rotates generators to deliver electricity. According to the rotating axis, there are two main types of turbine: Horizontal Axis Wind Turbines (HAWTs) and Vertical Axis Wind Turbines (VAWTs). The rotary axis of HAWTs is parallel to the wind direction, while that of VAWTs is perpendicular to the wind direction. Vertical-axis wind turbines are commonly used in residential areas, whereas horizontal-axis wind turbines are suitable for wind farms installed in rural areas or offshore. Vertical axis wind turbines do not need to be pointed into the wind direction to be more efficient [2], and they operate in the low-wind-speed environments [3]. The most commonly used VAWTs are Darrieus, Savonius, or hybrid turbines. The Darrieus turbine is a lift-based turbine, the Savonius is a drag-based turbine,

and the hybrid is predominantly lift-based turbine. The Savonius rotor was firstly developed and introduced by the Finnish inventor S.J. Savonius [4]. This wind turbine has been used in water pumping for agricultural applications [5], as an off grid power supply above communication towers [6], in standalone systems for domestic electricity generation [7], in street lighting systems [8], and as a windbreaker to improve the cooling efficiency in cooling towers [9].

Many scientists have studied the performance of the Savonius wind turbine in order to determine the optimum design parameters. A combination of Savonius and Darrieus turbines has been used to extract the exhaust systems of heat waste or natural heat sources [10,11]. The aerodynamic efficiency of different stages of the Savonius rotor has been investigated to determine its feasibility for the local production of electrical energy [12]. Blackwell et al. [13] showed that the two-stage geometry of the Savonius turbine has a better aerodynamic efficiency than the three-stage one. They also found that an increase in the aspect ratio improves the rotor performance. Alexander and Holownia [14] studied the effects of the blade aspect ratio, blade overlap, and gap as well as the effect of adding end extensions, end plates, and shielding. They showed that when the aspect ratio increases the efficiency, the rotor increases also. Modi et al. [15] found that the optimum values of the aspect and overlap ratios are 0.77 and 0.25, respectively. Mojola [16] showed that the effect of the overlap ratio is strongly influenced by the tip speed ratio of the rotor. The variation in fluid flow through Savonius turbines with different overlap ratios was investigated by Nobuyuki [17]. The performance of the Savonius rotor was greater for lower overlap ratios [18]. Saha et al. [19] reported that the optimum number of blades for the Savonius rotor is two. The curtain arrangement using one plate in the rotor-upper-end and the second plate at the rotor-lower-end was studied by Altan et al. [20]. They concluded that the arrangement increases the rotor efficiency. Gupta et al. [3] compared the results of Savonius–Darrieus wind turbine hybrid with those of the conventional Savonius rotor. They concluded that there is an improvement in the power coefficient for the hybrid Savonius–Darrieus rotor. Kamoji et al. [21] studied the effect of the overlap ratio, blade arc angle, aspect ratio, and Reynolds number on the performance of the Savonius rotor. They found that the modified Savonius turbine without an overlap ratio, with a blade arc angle of 124°, and with an aspect ratio of 0.7 has a maximum power coefficient of 0.21 at a Reynolds number of 150,000. Shankar [22] found that two-bladed Savonius rotors have an almost 50% higher peak power output than the three-bladed ones. Roy et al. [23] developed an inverse optimization methodology using differential evolution for a semicircular-bladed Savonius wind turbine. An investigation on two Savonius turbines by using PIV and CFD showed that the power enhancement is due to two factors: first, the Magnus effect and, second, the periodic flow between turbines [24]. Further investigation by [25-30] established parameters affecting the power enhancement such as the gap distance, turbine configuration, relative angular position, and rotor blade rotational direction. Meziane et al. [31] reported a rather extensive numerical investigation on three turbine clusters and a wind farm distribution. The challenge was to design and develop an optimal wind turbine cluster in order to extract the maximum amount of wind kinetic energy. The above studies on Savonius wind turbines gave different optimal design geometries.

As we can see from the previous literature review mentioned above, Savonius turbines have their own advantages. Naturally, we may ask if it is possible to improve efficiency by designing a Savonius power extraction turbine based on conventional rotor *without* requiring *complex modifications*? We have conducted some investigations about the influence of different parameters on energy extraction characteristics. All these investigations are based on numerical studies carried out using commercial CFD software and validated against experimental and numerical data derived from a literature review.

In addition, we conduct a comparative study between four different geometries (conventional two-bladed Savonius rotor, conventional three-bladed Savonius rotor, multiple semicircular two-bladed Savonius rotor and multiple semicircular three-bladed Savonius rotor). The aim of this work is to determine the optimal aerodynamic design with the highest power efficiency.

2. CFD model for analysis and design:

2.1. Description of the rotor design

Four different rotor blade configurations of the Savonius wind turbine were studied in this paper: conventional two-blade, conventional three-blade, multiple semicircular two-blade, and multiple semicircular three-blade. The conventional two-bladed Savonius turbine is described in reference [31], and its dimensions are listed in Table 1.

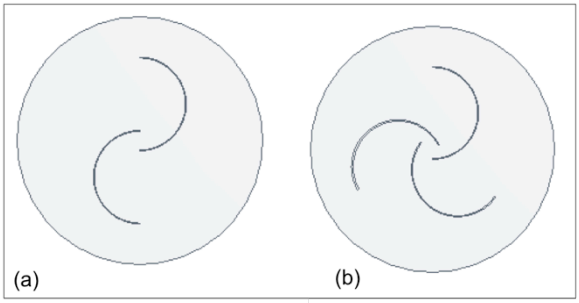

Fig. 1. Conventional (a) two-bladed and (b) three-bladed, Savonius wind turbines.

Fig.1 shows the geometry of the conventional Savonius rotor. It is a classical type of Savonius rotor, which consists of two and three semicircular blades. The overlap ratio of this turbine corresponds to the distance between the turbine blades divided by the blade chord and is equal to 0.20. The reason for choosing this overlap ratio is based on the need to conduct a validation study of the experimental results from reference [23]. Fig. 2 shows two new configurations on which we added two additional semi-circular blades inside both of the conventional configurations already presented in Fig.1.

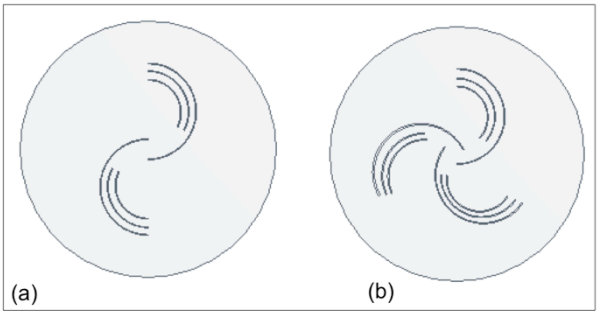

Fig. 2. Multiple semicircular (a) two-bladed and (b) three-bladed, Savonius wind turbines.

Table 1. Dimensions of the Savonius wind turbine.

Turbine type	Savonius wind turbine
Number of buckets	2.0
Blade diameter (m)	0.218
Aspect ratio	1.58
Blade chord (m)	0.109
Overlap ratio	0.20

2.2. Computational domain and boundary conditions

The computational domain was divided into two sub-domains: a circular moving domain containing the rotor, which rotates with the same angular velocity as the rotor, and a rectangular fixed domain, which determines the overall domain extent. The dimensions of the rectangular domain were selected in such a way that the results were not affected by the boundaries. A circular sliding interface was used to represent the connectivity between both domains. The rotating region was placed at 4D from the upper and lower sides of the whole domain, where a symmetry condition was defined. Steady-state flow conditions were assumed at the interface between the moving and stationary regions. Fig.3 shows the velocity profile and pressure distribution across the two sides of circular interface. It can be seen that the velocity profile and static pressure were the same at each grid of the interface zone.

The inlet velocities of 5.2, 6.2, 7.2, 8.2, 9.2, and 10.2 m/s and pressure outlet boundary conditions were placed respectively at a 4D distance upwind and 6D distance downwind with respect to the rotational axis of the wind turbine. The blades were considered to represent no slip boundary conditions in reference to the moving fluid zone. The same domain features were used for the simulation of all geometries.

2.3. Turbulence approach

The prediction of turbulent flows is an important step in the development of engineering problems involving flows. Based on the type of flow, different turbulence approaches have been adopted to lead to the closure of the equation system [32,33]. In a literature review, three different turbulence approaches were identified, each with advantages and disadvantages. Each of these approaches contributes to the prediction of low-speed or high-speed flows in a different way. The first approach is the direct numerical simulation (DNS), which offers a high-fidelity solution and uses a massive amount of computational resources. For this, the meshing size should be very small for very fine grids and the time history needs to be stored to make meaningful simulations. Very important time history data are generated at each time step, which is not necessary for the application under consideration. The second approach is the Large Eddy Simulation (LES), which needs less computational resources compared with the DNS. The LES method is based on the assumption that the relevant scales in turbulent flow can be separated into two different scale components: large and small scales. LES generates a large volume of time history data, which requires considerable analysis and a high CPU memory. The third approach is the Reynolds Averaged Navier–Stokes (RANS) method, which is the most common industrial tool in the prediction of low speed flows, as is the case in this work, due to the low computational requirements as compared with the DNS and LES. Some of the popular RANS based models are the k-ε, k-ω, and Shear Stress Transport (SST). These models provide accurate results while requiring low levels of computational resources.

In this work, five RANS turbulence models were examined using the same test case and compared with the experimental results of [23] at a tip speed ratio (TSR) of 0.55. The results of these runs can be found in Table 2. Using the SST model, the results of the CFD simulation were found to be in good agreement with the experimental results [30]. It is observed that the more the tip speed ratio increases, the greater the difference between the CFD simulation and experimental results is. Based on the results shown in Table 2 and from the available RANS models, the SST model was chosen for this study.

In this work, the coupled algorithm was employed for the pressure–velocity-coupling scheme in solution methods. The upwind differencing scheme was employed for spatial discretization of the momentum, turbulent kinetic energy, and turbulent dissipation rate.

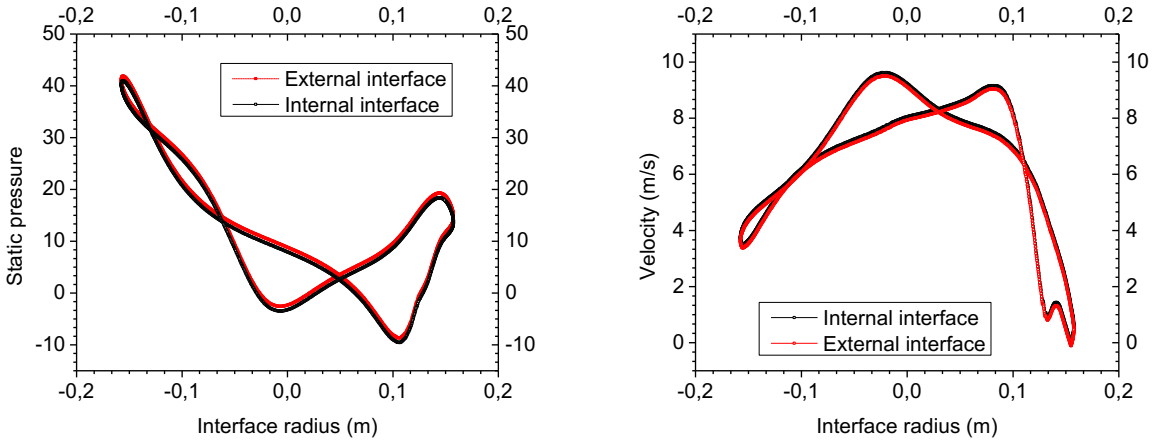

Fig. 3. Velocity profile and pressure distribution across the sides of the interface zone.

Table 2. Comparison of different turbulence models at a tip speed ratio (TSR) of 0.55

Reynolds Averaged Navier–Stokes (RANS) turbulence models	C_T (CFD)	C_T-(Saha et al.) (experimental)	% Difference
Standard k-ε	0.223	0.100	123 %
RNG k-ε	0.177	0.100	77 %
Realizable k-ε	0.212	0.100	112 %
Standard k- ω	0.209	0.100	109 %
Shear Stress Transport (SST) model	0.107	0.100	6.78 %

2.4. Mesh generation

In order to obtain a high level of performance and to prevent divergence caused by an unsuitable mesh refinement strategy, the effect of mesh refinement is being studied. A finer finite volume mesh commonly gives better calculation results. In this study, the computational domain was discretized with hybrid mesh. Triangle mesh was applied in most of the domain, and near the blades, it was refined with quadrilateral mesh to correctly predict the experimental results and capture the boundary layer viscous effects. A mesh sensitivity study was conducted to ensure the validation of the conventional two-bladed Savonius wind turbine. Six independent mesh tests were carried out until there were no significant changes in the evaluated variables (torque and power coefficients) of the conventional two-blade Savonius rotor. Table 3 shows the effect of the mesh dependency study on the torque coefficient evolution. Mesh independence was achieved for the 2D numerical simulation starting from almost 260,000 elements, since the torque coefficient value remained quasi-stable and its value was in good agreement with the experimental results [23]. The values of the torque coefficient became quasi stable between the two mesh elements at 260,000 and 725,000 where the error was 2.6%. From this, it can be concluded that 260,000 elements is independent, since the monitored values no longer change with increasing element numbers.

The growth rate was managed as 1.2 and 20 layers were imposed; therefore, the mesh density changed gradually, starting from the rotary domain and spreading to the stationary domain. Fig. 4 shows the mesh of the rotating domain and the refinement around the blades.

Table 3. Mesh sensitivity analysis for the conventional Savonius wind turbine at TRS = 0.75

Mesh	Number of cells	C_T-Conventional Savonius
1	60,350	0.312
2	138,000	0.293
3	260,000	0.227
4	330,000	0.223
5	520,000	0.226
6	725,000	0.221

Inflation layers were applied around the turbine blades to control cells close to them and to counter the change in the mesh size. At the interface between stationary and rotating domains, the mesh size had to be the same on both sides. Fig. 3 shows that the interface was well governed. Based on the velocity value, the non-dimensional wall distance ($y+$) value for the first mesh was approximately close to 1. The same mesh topology was repeated for all geometries. For mesh

convergence, $CFL = Udt/dx$ was used close to 1. Figs. 5 and 6 show the y+ variations for all Savonius rotors at a rotation angle of 160°. The first non-dimensional wall distance ($y+$) value was calculated using the following equation:

$$y^+ = \frac{\rho u_t dx}{\mu}$$

Where ρ represents the air density, u_t is the velocity friction, μ is the fluid viscosity, and dx is the distance from the blade surface.

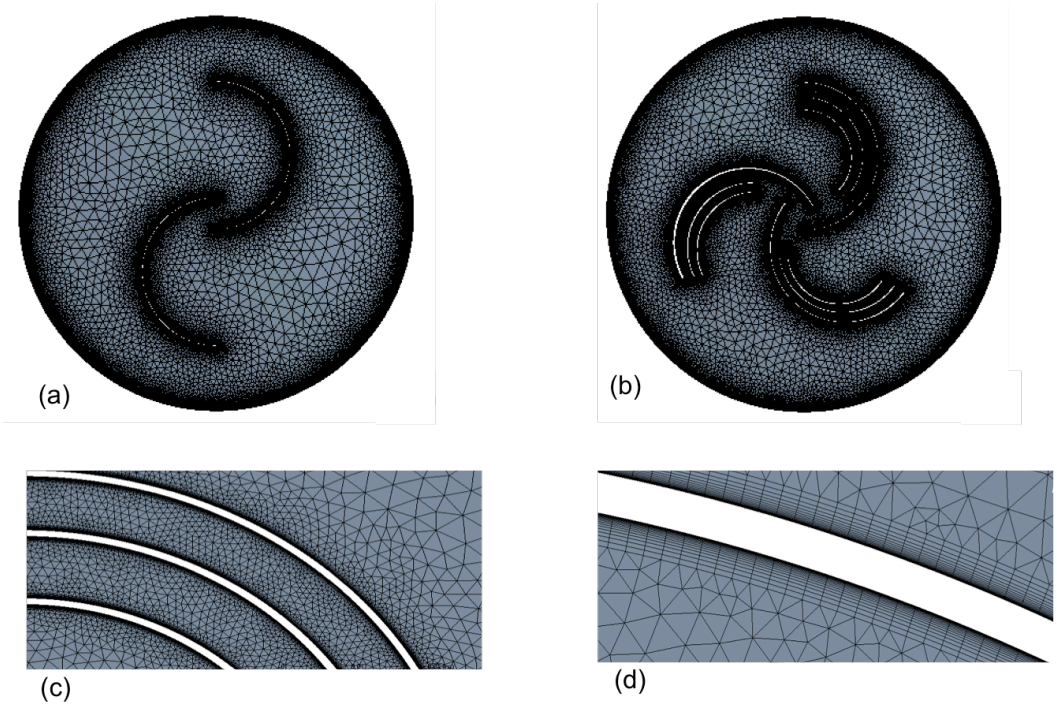

Fig. 4. Mesh of the rotating domain and interface boundary generated for (a) the conventional two-bladed rotor, (b) the multiple-semicircular three-bladed rotor, (c) the zoom view on additional multiple semicircular blades, and (d) the zoom view on one simple blade

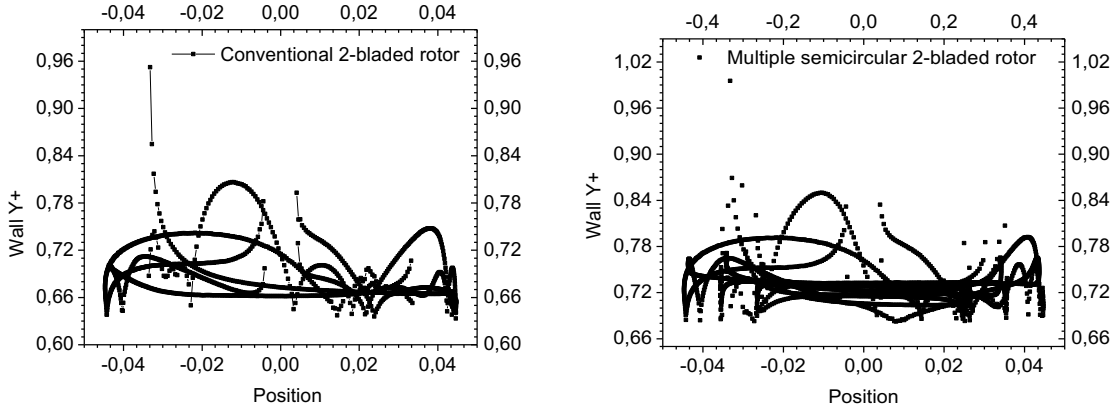

Fig. 5. Y+ on the two-bladed Savonius rotor at θ =160°.

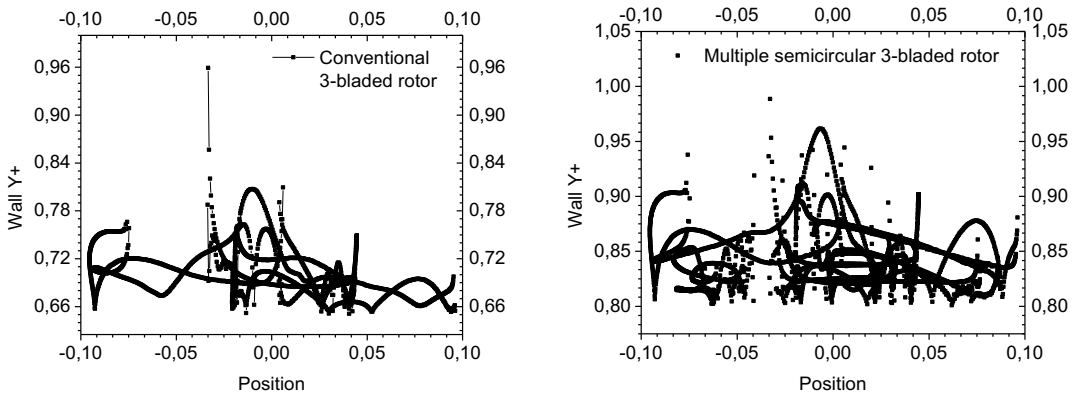

Fig. 6. Y+ on the three-bladed Savonius rotor at θ =160°.

The torque coefficient (C_T), power coefficient (C_P), and tip speed ratio (TSR) of this Savonius wind turbine were calculated in terms of the following equations:

$$C_T = \frac{T}{0.5\,\rho A U^2 R}$$

$$C_P = \frac{P_{turbine}}{P_{Wind}} = \frac{T\,\omega}{0.5\,\rho A U^3}$$

$$TSR = \frac{\omega\,R}{U}, \qquad and \qquad \omega = \frac{2\pi N}{60}$$

Where C_T is the torque coefficient, C_P is the power coefficient, $P_{turbine}$ is the power produced by the turbine, P_{Wind} is the kinetic energy of air, T is the torque acting on the turbine, ρ is the air density, A is the swept area of the turbine, U is the air speed, ω is the angular velocity of the turbine, R is the rotor radius, and N represents the rpm of the rotor

3. Results and discussion

Multiple studies have been conducted on the Savonius wind turbine design and efficiency. These studies have presented the effects of various parameters such as the aspect ratio and overlap ratio and blade design improvement for the conventional semicircular Savonius configuration. In the present study, two new configurations with multiple additional blades were compared with the conventional two and three Savonius rotors. A validation study was performed on the conventional configuration by comparing the numerical results with the experimental data [23]. The torque coefficient (C_T) and power coefficient (C_P) were calculated for each configuration over a set of operational TSRs for six turbines to provide a numerical platform for a comparative study. Mesh sensibility analyses were also performed for each case to assess the quality of the results and to predict the experimental data correctly.

3.1. Performance analysis and validation study

Table 4 shows a comparison of the power and torque coefficients as a function of the TSR of the conventional two-bladed Savonius wind turbine between the CFD model and experimental data [23]. Good agreement was observed between the results, since the C_P and C_T trends appear to be well predicted by the CFD model. Furthermore, at a low TSR, there was no significant difference between the results. At a high TSR, the difference between numerical and experimental data became more significant (around 18%), but the trends were highly comparable. This difference can be explained by the use of the SST model for turbulence modeling, since this model exhibits lower sensitivity to free stream conditions [34].

Table 4. Comparison between the numerical simulation and experimental data [23].

TSR	CP- (CFD)	CP- (Saha et al.)	CT- (CFD)	CT- (Saha et al.)	% Difference
0.55	0.059	0.055	0.107	0.100	6.78 %
0.6	0.078	0.072	0.130	0.120	7.69 %
0.65	0.124	0.110	0.191	0.169	11.29 %
0.7	0.163	0.142	0.233	0.203	12.88 %
0.75	0.167	0.140	0.223	0.187	16.16 %
0.8	0.138	0.112	0.172	0.140	18.84 %

3.2. Optimal design and performance analysis:

The influence of additional multiple semicircular blades on the efficiency of the Savonius rotor was studied in this work. Numerical simulations were conducted by adding multiple semicircular blades to conventional Savonius rotors.

The evolution of the torque coefficient (C_T) and power coefficient (C_P) with the TSR for the four rotor geometries is shown in Figs. 7 and 8. These figures show that when the number of blades on the conventional rotor increased from two to three, the values of C_P and C_T decreased greatly by almost 9%. The value of C_P decreased due to an increase in the rotor's inertia. In the case of two-bladed conventional rotor, an average improvement of 8.43% was observed in rotor efficiency when the multiple additional two-blade structure was adopted. Figs. 7 and 8 show similar trends for torque and power coefficients for all rotor configurations, and it can be seen that the gap of C_P and C_T for all rotor geometries increased with the TSR. The maximal values of C_P and C_T were found for the multiple semicircular two-bladed Savonius rotor. These values were 0.2075 and 0.277, respectively, and they corresponded to a TSR of 0.75, showing an improvement of 10.7%. The maximal operating regime was achieved when the TSR was equal to 0.75, since the different rotors achieved their peak efficiency at this TSR. For better accuracy and precision, the comparison of C_P and C_T was done after four complete revolutions.

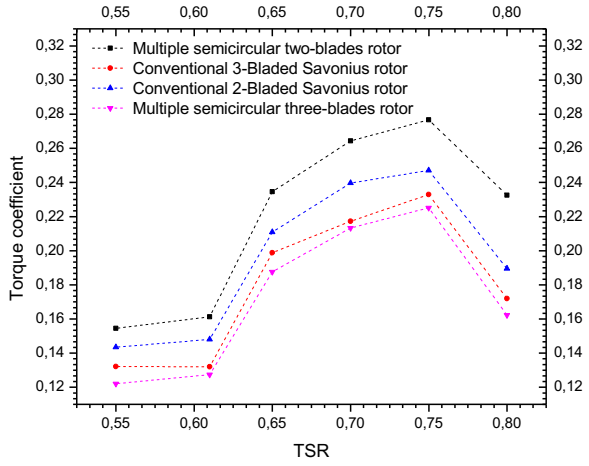

Fig. 7. Evolution of the torque coefficient with the TSR for different rotor configurations.

The torque coefficient for the different rotor configurations was evaluated at each rotation degree for different TSR cases. Each time step corresponded to one degree of the rotating zone. The comparison of torque coefficient evolution with angle of rotation for the conventional two-bladed rotor, conventional three-bladed rotor, multiple semicircular two-bladed Savonius rotor, and multiple semicircular three-bladed Savonius rotor is shown in Figs. 9–11 for TSR values equal to 0.55, 0.6, 0.65, 0.70, 0.75, and 0.80, respectively. Figs. 12–13 show the evolution of the power coefficient with an angle of rotation of the conventional two-bladed rotor and its modified multiple-blade configuration. It can be seen that the difference between torque coefficients increased with the TSR. When the exposed area on the advancing blade increased, the available air kinetic energy of the incoming fluid also increased, which contributed to the positive torque.

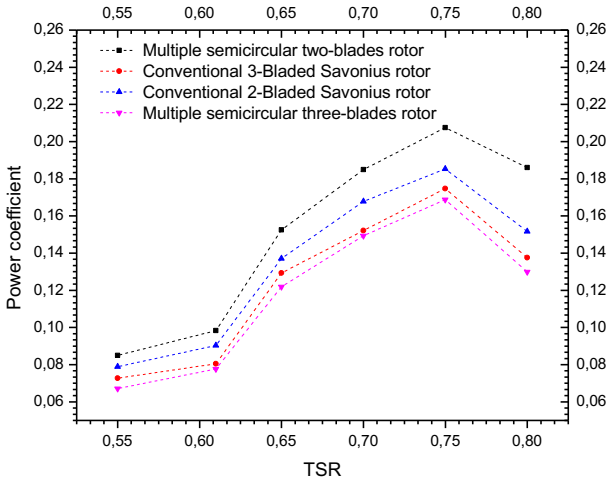

Fig. 8. Evolution of the power coefficient with the TSR for different rotor configurations.

Fig. 14 shows the velocity contours for all rotor configurations taken into account in this study and operating at three different tip speed ratios (0.55, 0.65, and 0.75). For better accuracy and precision, the results are presented after four complete revolutions of the rotor. After four revolutions, the flow distribution around the blades became stable and we could not observe any significant change in the flow architecture. As we can see from Fig. 14, the convex surface of the blade is under relatively low pressure and the concave surface is under relatively high pressure. The pressure difference between the concave and convex surfaces is very small so that the energy extraction efficiency of the lift force in this case is very limited.

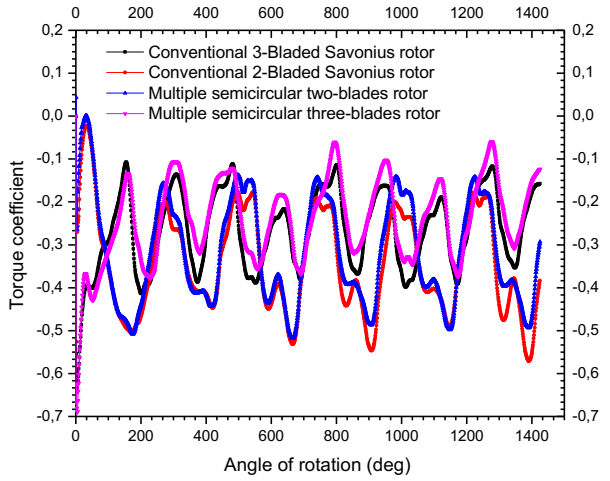

Fig. 9. Evolution of the torque coefficient with the angle of rotation for a TSR of 0.55.

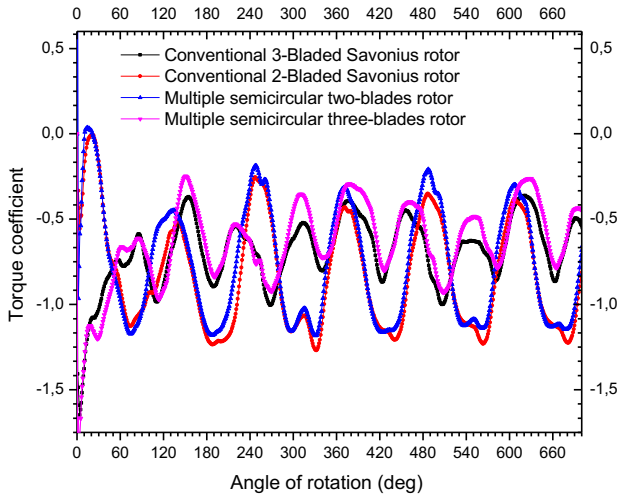

Fig. 10. Evolution of the torque coefficient with the angle of rotation for a TSR of 0.7.

It can be seen that the fluid around the rotating zone started to rotate due to the rotating motion of the rotor, and the curvature shape of the blades helped to extract the maximal air kinetic energy because of the favorable pressure gradient over the blades. Vortices, dead zones, and shear flow took place around the surface of the blade due to the boundary layer separation and no-slip boundary conditions. The developed vortices were carried downstream into the viscous wake. Other types of fluid phenomena (Coanda effect, pressure difference, etc.) were observed close to the blades.

The incoming flow changed its direction tangentially towards the rotating fluid motion and prevented the impact of the fluid on the advancing and returning blades of the rotor.

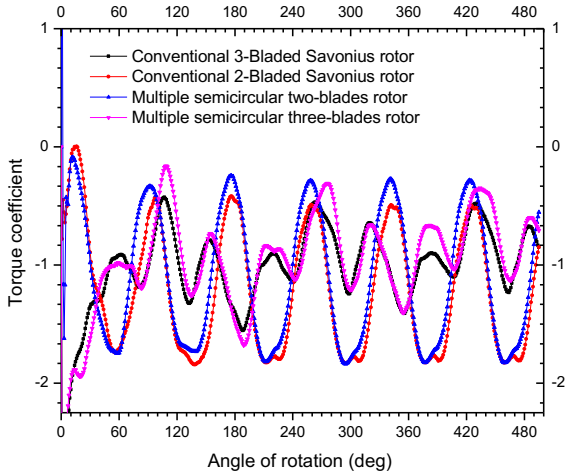

Fig. 11. Evolution of the torque coefficient with the angle of rotation for a TSR of 0.8.

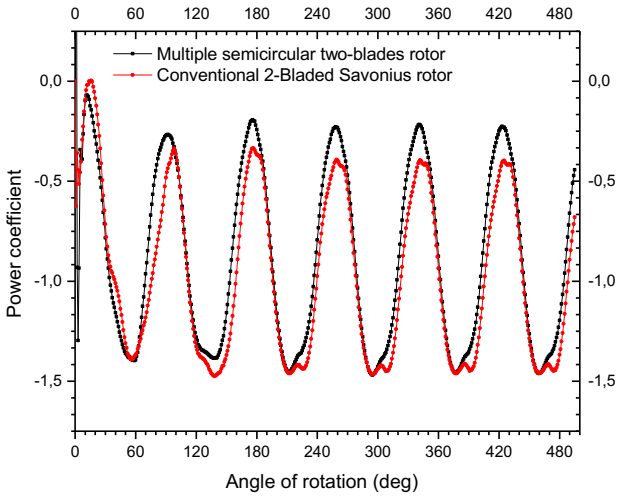

Fig. 12. Evolution of the power coefficient with the angle of rotation for a TSR of 0.8.

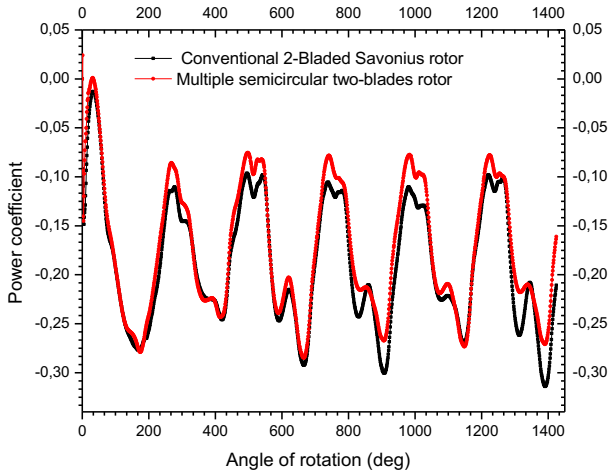

Fig. 13. Evolution of the power coefficient with the angle of rotation for a TSR of 0.55.

To achieve an optimum power and aerodynamic efficiency, the manufacture of the design using aluminum alloy was proposed because of its lightweight, high stiffness, and low cost.

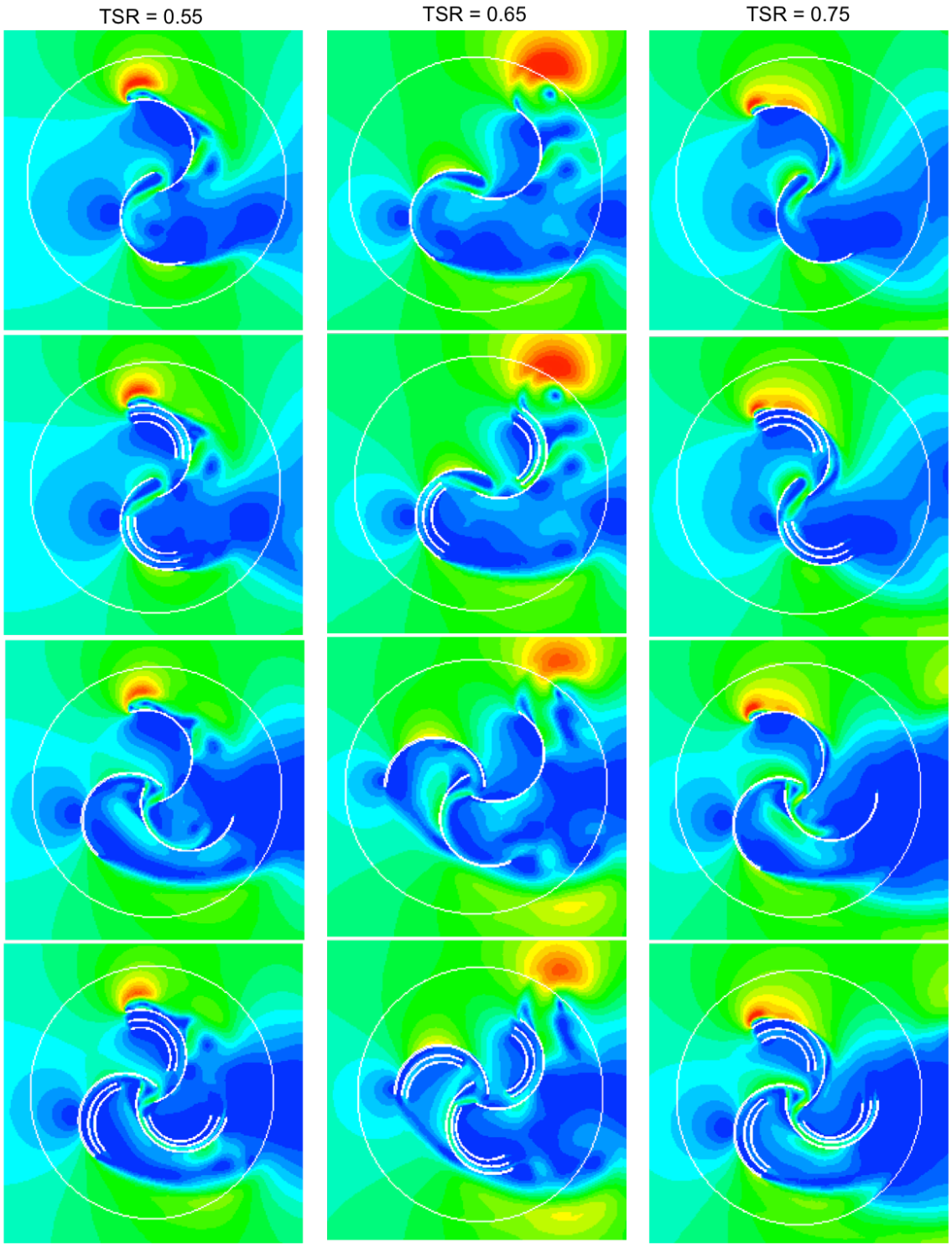

Fig. 14. Velocity contours of conventional two-bladed, conventional three-bladed, and multiple semicircular two- and three-bladed Savonius rotors.

4. Conclusion

In this study, the authors developed an unsteady 2D numerical model in order to simulate and evaluate the effect of adding multiple semicircular blades on the efficiency of conventional two-bladed and three-bladed Savonius wind turbine rotors. The model was implemented in Ansys Fluent and validated against experimental data obtained in the subsonic wind tunnel owned by the Institute of Technology Guwahati based on a literature review.

The goal was to develop an innovative and efficient Savonius wind turbine system. Various empiric turbulence models were tested in this study to determine the right one

for this study. The SST turbulence model, which is the combination of the k-ε and k-ω models, was able to predict the experimental results with a high level of accuracy. A mesh sensitivity study was conducted to obtain the optimal mesh elements with a lower computational cost. Mesh independence was achieved starting from 260,000 elements, since the torque coefficient value remained stable. In order to capture the flow phenomena (Coanda effect, recirculation area, vortex, etc.) near the rotor blades, due to the interaction between the rotor walls and airflow, we used inflation layer meshing to accurately capture the boundary layer zone for any blade wall turbulent flow.

- The comparison between four rotor configurations showed that the multiple semicircular two-blade Savonius rotor is more efficient than other configurations. The comparison was done for six different operating TSRs.
- The maximum torque coefficient and power coefficient were 0.207 and 0.277, respectively, and these corresponded to a TSR of 0.75, showing an improvement of 10.7% compared with the conventional two-bladed rotor.
- This work proves that the Savonius rotor can exhibit enhanced efficiency with a simple design modification.
- The advantage of this design is that it can be used to build an efficient Savonius wind turbine without increasing the rotor diameter or making any complex changes in the rotor design.

In summary, the modification of vertical axis turbine with the two semicircular blades proposed in this work can effectively improve energy extraction efficiency, which provides a new idea for the design of high-efficiency vertical axis turbines. Future work will investigate ways to improve the self-starting ability of hybrid multiple-semicircular Savornius and Darrieus rotors with simple modifications.

References

[1] G.W.E.C., 2018. Global wind report: annual market update 2018.

[2] S. Roy, A. Ducoin, "Unsteady analysis on the instantaneous forces and moment arms acting on a novel Savonius-style wind turbine", Energy Convers Manage, vol. 121, pp. 281–296, 2016.

[3] R. Gupta, A. Biswas, "CFD analysis of flow physics and aerodynamic performance of a combined three-bucket Savonius and three-bladed Darrieus turbine", Int J Green Energy, Vol. 8, pp. 209–233, 2011.

[4] R. Gupta, A. Biswas, KK. Sharma, "Comparative study of a three-bucket Savonius rotor with a combined three-bucket Savonius-three-bladed Darrieus rotor", Renew Energy, Vol. 33, pp.1974–1981, 2008.

[5] A. Zingman, "Optimization of a Savonius rotor vertical-axis wind turbine for use in water pumping systems in rural Honduras". SB thesis no. 212409044-MIT. Cambridge (USA): Massachusetts Institute of Technology; 2007.

[6] BD. Plourde, JP. Abraham, GS. Mowry, WJ. Minkowycz, "Simulations of three-dimensional vertical-axis turbines for communications applications", Wind Eng, Vol. 36, no. 4, pp. 354–443, 2012.

[7] I. Al-Bahadly, "Building a wind turbine for rural home", Energy Sustain Dev, Vol. 13, no. 3, pp. 159–165, 2009.

[8] R. Ricci, R. RomagnolI, S. Montelpare, D. Vitali, "Experimental study on a Savonius wind rotor for street lighting systems", Appl Energy, Vol. 161, pp. 143–152, 2016.

[9] M. Goodarzi, R. Keimanesh, "Numerical analysis on overall performance of Savonius turbines adjacent to a natural draft cooling tower", Energy Convers Manage, Vol. 99, pp. 41–49, 2015.

[10] S. Bhuyan, A. Biswas, "Investigations on self-starting and performance characteristics of simple H and hybrid H-Savonius vertical axis wind rotors", Energy Convers Manage, Vol. 87, pp. 859–867, 2014.

[11] M. Meziane, M. Faqir, E. Essadiqi, MF. Ghannameh, "Numerical Investigation of Hybrid Darrieus-Savonius Wind Turbine Performance", In: Proceedings of the international Conference on Advanced Intelligent Systems for Sustainable Development AI2SD'2019, 08–11 July. Marrakech, Morocco; 2019.

[12] J.L. Menet, "A double-step Savonius rotor for local production of electricity: a design study", Renew. Energy, Vol. 29, pp. 1843–1862, 2004.

[13] B.F. Blackwell, R.E. Sheldahl, L.V. Feltz, "Wind Tunnel Performance Data for Two- and Three-bucket Savonius Rotors", Thesis Issued by Sandia Laboratories, July 1977.

[14] A.J. Alexander, B.P. Holownia, "Wind tunnel tests on a Savonius rotor", Journal of Industrial Aerodynamics, Vol. 3, pp. 343–351, 1978.

[15] V.J. Modi, N.J. Roth, M.S. Fernando, "Optimum-configuration studies and prototype design of a wind-energy-operated irrigation system", Journal of Wind Engineering and Industrial Aerodynamics, Vol. 16, pp. 85–96, 1984.

[16] O. Mojola, "On the aerodynamic design of the Savonius windmill rotor", Journal of Wind Engineering and Industrial Aerodynamics, Vol. 21, pp. 223–231, 1985.

[17] F. Nobuyuki, "On the torque mechanism of Savonius rotors", Journal of Wind Engineering and Industrial Aerodynamics, Vol. 40, pp. 277–292, 1992.

[18] N. Fujisawa, "On the torque mechanism of Savonius rotors", J Wind Eng Ind Aerodyn, Vol. 40, pp. 277–292, 992.

[19] U.K. Saha, S. Thotla, D. Maity, "Optimum design configuration of Savonius rotor through wind tunnel experiments", Journal of Wind Engineering and Industrial Aerodynamics, Vol. 96, pp. 1359–1375, 2008.

[20] B.D. Altan, M. Atılgan, "An experimental study on improvement of a Savonius rotor performance with curtaining", Experimental Thermal and Fluid Science, Vol. 32, pp. 1673–1678, 2008.

[21] M.A. Kamoji, S.B. Kedare, S.V. Prabhu, "Experimental investigations on single stage modified Savonius rotor", Applied Energy, Vol. 86, pp. 1064–1073, 2008.
[22] P.N. Shankar, "Development of vertical axis wind turbines", in: Proc. Indian Acad. Sci., vol. C 2, pp. 49–66; March 1979.
[23] S. Roy, R. Das, U.K. Saha, "An inverse method for optimization of geometric parameters of a Savonius style wind turbine", Energy Conversion and Management, Vol. 155, pp. 116–127, 2018.
[24] Y. Shigetomi, Y. Murai and Y. Tasaka, "Interactive flow field around two Savonius turbines", Renewable energy, vol. 36, no. 2, pp. 536-545, Feb 2011.
[25] B. Belkacem and M. Paraschivoiu, "CFD Analysis of a Finite Linear Array of Savonius Wind Turbines", In Journal of Physics: Conference Series, vol. 753, no. 10, pp. 102008, Sep 2016.
[26] Ö. Kiymaz and T. Yavuz, "Wind power electrical systems integration and technical and economic analysis of hybrid wind power plants," 2016 IEEE International Conference on Renewable Energy Research and Applications (ICRERA), Birmingham, pp. 158-163, 2016.
[27] A. Harrouz, I. Colak and K. Kayisli, "Energy Modeling Output of Wind System based on Wind Speed," 2019 8th International Conference on Renewable Energy Research and Applications (ICRERA), Brasov, Romania, pp. 63-68, 2019.
[28] A. Harrouz, I. Colak and K. Kayisli, "Control of a small wind turbine system application," 2016 IEEE International Conference on Renewable Energy Research and Applications (ICRERA), Birmingham, pp. 1128-1133, 2016.
[29] J. Song, S. J. Song, S. Oh and Y. Yoo, "Optimal operational state scheduling of wind turbines for lower battery capacity in renewable power systems in islands," 2016 IEEE International Conference on Renewable Energy Research and Applications (ICRERA), Birmingham, pp. 164-168, 2016.
[30] M. Karimirad and K. Koushan, "WindWEC: Combining wind and wave energy inspired by hywind and wavestar," 2016 IEEE International Conference on Renewable Energy Research and Applications (ICRERA), Birmingham, pp. 96-101, 2016.
[31] M. Meziane, E. Essadiqi, M. Faqir, and M.F. Ghanameh, "CFD Study of Unsteady Flow Through Savonius Wind Turbine Clusters", International Journal of Renewable Energy Research , vol. 9, no. 2 pp. 657-666, Jun 2019.
[32] M. Meziane, O. Eichwald, J.P. Sarrette, O. Ducasse and M. Yousfi, "2D simulation of active species and ozone production in a multi-tip DC air corona discharge", Eur. Phys. J. Appl. Phys. Vol. 56, no. 2, 2011.
[33] M. Meziane, O. Eichwald, J.P. Sarrette, O. Ducasse and M. Yousfi, "Multi-dimensional simulation of a polluted gas flow stressed by a DC positive multi-pins corona discharge reactor", International Journal of Plasma Environmental Science & Technology, Vol. 6, no.2, 2012.
[34] MH. Mohamed, G. Janiga, E. Pap, D. Thévenin, "Optimal blade shape of a modified Savonius turbine using an obstacle shielding the returning blade", Energy Convers Manage, Elsevier Ltd, Vol. 52. pp. 236–242, 2011.